Publisher: GSA
Journal: GEOL: Geology
DOI:10.1130/G36489.1

Nano-scale records of ancient shock deformation: Reidite ($ZrSiO_4$) in sandstone at the Ordovician Rock Elm impact crater

Aaron J. Cavosie[1,2,3], Timmons M. Erickson[1], and Nicholas E. Timms[1]

[1]*Department of Applied Geology, Curtin University, Perth 6102, Australia*

[2]*Department of Geoscience, University of Wisconsin-Madison, Madison, Wisconsin 53706, USA*

[3]*Department of Geology, University of Puerto Rico-Mayagüez, Mayagüez, Puerto Rico 00681, USA*

ABSTRACT

The terrestrial record of meteorite impacts is difficult to decipher because unequivocal evidence of impact is increasingly destroyed with time by erosion, burial and tectonics. Zircon survives these processes as a shocked mineral, and above 20 GPa transforms to reidite, a high pressure $ZrSiO_4$ polymorph diagnostic of impact. However, the utility of reidite has been limited by its occurrence; it has only been reported from three relatively young (<36 Myr) impact craters globally. Here we report a new occurrence of reidite in brecciated sandstone from the Ordovician Rock Elm impact crater in Wisconsin, USA. Electron backscatter diffraction mapping was used to identify reidite and microtwins within shocked zircons smaller than 50 μm in diameter. Reidite occurs as both 200–500 nm wide lamellar intergrowths and as nanoparticulate grains, which not only provide the first diagnostic evidence for ultra-high-pressure shock metamorphism at Rock Elm, but is also the oldest reported occurrence of reidite. Considering its small size, and the ubiquitous presence of detrital zircon in siliciclastic rocks, reidite may be more common in the rock record but has potentially gone undetected. The recognition that nano-scale reidite can be preserved over deep time within zircon in shock-metamorphosed sandstone presents new

Publisher: GSA
Journal: GEOL: Geology
DOI:10.1130/G36489.1

opportunities for investigating Earth's impact record, as it could potentially preserve nanoscopic evidence of impact events much older than Rock Elm. Given that shocked zircons have been shown to survive sedimentary cycling, the identification of reidite within zircons in siliciclastic rocks could facilitate investigating the impact chronology over much of the geological time scale, as the oldest terrestrial minerals known are detrital zircons.

INTRODUCTION

Reidite is a tetragonal $ZrSiO_4$ polymorph with scheelite structure (space group $I4_1/a$) that was first reported from high-pressure experiments (Reid and Ringwood, 1969). A range of experimentally determined pressures for zircon-reidite equilibrium at ambient temperature have since been reported (e.g., Kusaba et al., 1985; Knittle and Williams, 1993). At high temperatures reidite is unstable; it reverts to zircon above 1200 °C (Kusaba et al., 1985). Naturally occurring reidite forms when zircon is shock metamorphosed (Glass et al., 2002), and has only been reported from three impact structures where it occurs in ejecta and melt-bearing breccia. Reidite was first described in distal ejecta from the 35.5 Ma Chesapeake Bay impact structure, USA (Glass and Liu, 2001; Wittmann et al., 2009). It has since been found at the 15.1 Ma Ries crater in Germany (Gucsik et al., 2004; Wittmann et al., 2006), and at the 0.05 Ma Xiuyan crater in China (Chen et al., 2013). Of significance to this study is that in crater environments, reidite has only been found in crystalline clasts incorporated in impact melt-bearing breccia; it has not been reported in other target lithologies. Here we report an occurrence of sub-μm reidite in sandstone breccia from Rock Elm, a deeply eroded, Middle Ordovician impact structure in Wisconsin, USA. These results are the first documented occurrence of reidite in a sedimentary target rock, and constitute the oldest known reidite in the geological record.

GEOLOGICAL BACKGROUND

Rock Elm is a 6.5 km diameter impact crater in Paleozoic target rocks in western Wisconsin, USA (Fig. 1A). The complex impact crater is formed in Upper Cambrian and Early Ordovician sedimentary rocks, with an impact age of 470–450 Ma constrained by unconformably overlying Middle Ordovician basin fill sediments (Cordua, 1985; French et al., 2004). The central uplift consists of a ~1 km diameter circular area of poorly exposed isolated blocks of bedded sandstone and conglomerate interpreted to be the Mt. Simon Formation, an Upper Cambrian cratonic sequence that is dominantly mature quartz arenite (Lovell and Bowen, 2013). Breccia from the central uplift has been described (Cordua, 1985; French et al., 2004), however no in situ outcrops have been reported. The breccia is comprised of lithic clasts of variable size and composition within a matrix of sand-sized particles. French et al. (2004) reported shocked quartz grains with planar fractures that indicate pressures of 5–10 GPa, confirming an impact origin for the Rock Elm breccia.

SAMPLE AND METHODS

Breccia sample 13RE07 was collected in 2013 as a ~25 cm loose block from a low mound (10 cm high) of soil and rock fragments in the central uplift (GPS coordinates: N44° 43.027’; W92° 13.822’). The breccia contains deformed < 0.5 cm mixed sedimentary lithic clasts, shocked quartz and minor alkali feldspar sand grains in an opaque reddish matrix, with voids ranging from sand-sized porosity to 3-cm vugs (Fig. 1B). Shocked quartz grains contain one to four orientations of parallel planar fractures (Fig. 1C), similar to those described by French et al. (2004). A total of 135 zircons larger than 10 μm in diameter were documented in one polished petrographic thin section using scanning electron microscopy (SEM); most preserve oscillatory growth zoning, occur in the matrix, and are interpreted as detrital in origin. Electron backscatter diffraction (EBSD) mapping revealed the presence of reidite in two zircons within a

3.5 × 0.5 mm clast, and a zircon with microtwins nearby in the matrix. For details of the methods and analytical conditions, see the GSA Data Repository[1].

RESULTS

Shock-Twinned Zircon

Zircon 36 (Fig. 2A) is a 10 × 15 μm anhedral fragment. High spatial resolution EBSD mapping using 50 nm step size identified five parallel sub-μm wide microtwin lamellae on the right side of the grain (green in Fig. 2A). The microtwins are related to the host zircon by 65° misorientation about <110>, which results in the sharing of a {112} orientation between the two domains (see the Data Repository). Despite occurring in an area of high fracture density, the microtwins are not visible in atomic number contrast imaging (see the Data Repository).

Reidite-Bearing Zircons

Zircon 9 is a 30 × 40 μm subhedral grain with irregular form. The upper margin is cuspate and contains narrow tubular embayments, the right side of the grain preserves prism and pyramid faces, and the left side appears to have partially disaggregated (Figs. 2B, 3A). The host grain preserves crystallographic misorientation of up to 25 degrees from the mean orientation, principally as a combination of sub-planar deformation bands and isolated fragments (Fig. 3C). The dispersion of crystallographic poles for the host grain has a complex pattern, but is predominantly around <001> (Fig. 3E). The misorientation of isolated blocks likely results from rigid rotation due to fracturing, whereas deformation bands are low-angle boundaries formed by the stacking of dislocations. The <001> parallel misorientation axis is consistent with dislocation slip by {100}<010> (Leroux et al., 1999; Timms et al., 2012).

Two sets of parallel sub-μm lamellae on the right side of the grain are brighter in atomic number contrast imaging than the host zircon, yield elemental spectra (by energy dispersive spectroscopy) consistent with $ZrSiO_4$, and produce EBSD patterns that index as reidite (Figs. 2B, 3). The lamellae are non-luminescent in cathodoluminescence, and cross-cut growth zoning in the host zircon (see the Data Repository). The lamellar reidite occurs in two distinct planes (1 and 2 in Fig. 3D) and shows systematic relationships with the host zircon. Reidite crystallographic poles show tight clusters, such that each lamellae set shares its (001) with a different {110} in the host zircon, and a {110} for each reidite set aligns with (001) of the host zircon (Fig. 3E).

In addition to lamellae, a nanoparticulate form of reidite is present lining the outer margin of the grain and within irregular, cuspate voids within the host zircon (Figs. 2B, 3D). These grains were calculated to have a mean diameter of 192 nm (±115 nm, one standard deviation). Crystallographic analysis shows a scattered orientation distribution, where the poles of (001) only broadly cluster around poles to {110} in the host zircon; a significant portion of the nano-reidite grains show no systematic relationship to the zircon (Fig. 3E).

Zircon 10 is a 40 × 50 µm blocky subhedral zircon that contains reidite in three small domains (Fig. 2C). EBSD mapping of the largest domain (~0.5 × 2 µm) shows that the reidite is in a single orientation, and has the same relationship to the host grain as zircon 9 (see Data Repository). The small size precludes identification of habit, although an array of grains in uniform orientation is consistent with lamellar form.

DISCUSSION

Electron Backscatter Diffraction: A New Method to Identify Reidite

Reidite has previously been documented in shocked zircon using transmission electron microscopy (TEM) (Leroux et al., 1999), X-ray diffraction (Glass and Liu, 2001), and Raman spectroscopy (Wittmann et al., 2006; Chen et al., 2013). As shown here, EBSD is an additional method for identifying reidite, and can provide highly spatially resolved crystallographic data collected in situ from sub-μm domains in a thin section. The Rock Elm data confirm crystallographic relations between zircon and reidite determined previously in experimentally shocked grains measured by TEM, where $\{100\}_{Zrn}//\{112\}_{Red}$, and $[001]_{Zrn}//<110>_{Red}$ (Leroux et al., 1999).

An Occurrence of Sub-μm Granular Reidite

Sub-micrometer granular reidite has not previously been described in nature, however, it has been documented in zircon experimentally shocked at 60 GPa (Leroux et al., 1999). The various occurrences of nano-scale granular reidite in zircon 9 (Fig. 3D) are remarkably similar, whether on exterior surfaces, lining cuspate margins and interior voids, or lining nearby disaggregated zircon fragments. The presence of two distinct occurrences of reidite within a single shocked zircon implies that multiple transformation mechanisms operated simultaneously, or alternatively, that two separate shock events are recorded in this grain. Either scenario is constrained to have occurred over the millisecond timescales that high-pressure conditions were present during the passage of the shockwave (Melosh, 1989). The lamellar form of reidite and its topotactic relation with the host zircon is consistent with a shear-dominated phase transformation (Kusaba et al., 1986), whereas the formation mechanism of the nano-granular reidite appears most consistent with a reconstructive transformation mechanism that relies on nucleation and growth of new grains from the host zircon (Dutta and Mandal, 2012). Further exploring the variable response of zircon during dynamic high pressure polymorphism is beyond the scope of this contribution, and is the focus of ongoing work.

Shock History of the Rock Elm Breccia

An inherent difficulty in field investigations of Rock Elm breccia is the inability to observe contact relations with the Mt. Simon sandstone. Regardless, the presence of shocked quartz (French et al., 2004; Fig. 1C), and the shock-twinned zircon and reidite reported here provide incontrovertible evidence of high pressure deformation that links breccia formation to the impact. The conditions under which deformation twins form in zircon have not been experimentally determined, however shock-twinned zircon has only been reported from impact environments (Moser et al., 2011; Timms et al., 2012; Erickson et al., 2013a, 2013b, Thomson et al., 2014). In experiments, planar microstructures are pervasive at 20 GPa (Leroux et al., 1999), and so it follows that shock-twinned zircons record at least 20 GPa. Reidite represents the highest pressure phase thus far identified at Rock Elm. While stable at pressures as low as 20 GPa in static experiments (Knittle and Williams, 1993; van Westrenen et al., 2004), in shock recovery experiments reidite forms between 30 and 40 GPa (Kusaba et al., 1985; Leroux et al., 1999). In crater environments, reidite has only been reported in melt-bearing impact breccias (Wittmann et al., 2006; Wittmann et al., 2009; Chen et al., 2013) that record shock stage II to III conditions, corresponding to pressures from 35 to 60 GPa (Stöffler and Grieve, 2007). We thus tentatively assign shock stage II conditions (35–45 GPa) to breccia sample 13RE07, as it is the minimum stage for which the conditions necessary to form reidite occur (Stöffler and Grieve, 2007).

A New Locality and the Oldest Occurrence

Rock Elm represents the fourth impact structure where reidite has been documented, and with a minimum age of 450 Ma (French et al., 2004) is by far the oldest reidite known. Of the 185 confirmed impact structures in the Earth Impact Database (Spray and Elliot, 2015), 154 craters (83%) are younger than Rock Elm, and thus could feasibly preserve reidite if zircons

DOI:10.1130/G36489.1

were present in the target rocks. Reidite has not been reported from the largest known terrestrial impact structures, such as the Vredefort Dome and Sudbury, where large volumes of rock were exposed to higher shock pressures than Rock Elm. One possible reason for the paucity of reidite at these sites may be the rapid reversion to zircon at temperatures above 1200 °C (Kusaba et al., 1985). Post-impact thermal conditions may inhibit wide-spread preservation of reidite in basement rocks at large impact structures. Reidite may thus be preferentially preserved in impact breccias typically found in the higher levels of impact structures, such as at Ries (14.5 Ma, 24 km) and Chesapeake Bay (35.5 Ma, 85 km), and also at relatively small and/or young impact craters, as exemplified by Xiuyan (0.05 Ma, 1.8 km).

Implications for Preservation of Reidite in Sediments and Rocks

Given the ubiquitous occurrence of detrital zircon in siliciclastic rocks, these findings highlight the preservation potential of reidite in shocked sandstone, a reservoir not generally recognized for preservation of ultra-high pressure shock records. For ancient impact structures that have since eroded, reidite may be preserved in detrital shocked zircons that have been eroded and transported, and now reside in younger sedimentary rocks. Shocked zircons with diagnostic shock microstructures are ubiquitous in modern alluvium eroded from complex craters, such as the Vredefort Dome (Cavosie et al., 2010; Erickson et al., 2013b), Sudbury (Thomson et al., 2014), and Santa Fe (Lugo and Cavosie, 2014) impact structures. With the recognition that Hadean detrital zircons with ages up to 4.4 Gyr are preserved (Valley et al., 2014), reidite may also provide a record of even earlier impact bombardment. Identification of reidite in ancient detrital zircons could provide ground-truth evidence from the terrestrial record of early impact events on Earth.

ACKNOWLEDGMENTS

N.K. provided access to the site. P. Montalvo, C. Lugo, D. Colon, and C. Roig provided field assistance. J. Anderson, P. Bland, W. Cordua, B. Hess, M. Spicuzza, and J. Valley are thanked for discussions and assistance. We thank W. Cordua, A. Wittmann, and an anonymous reviewer for constructive suggestions. Support was provided by NSF (EAR-1145118), NASA Astrobiology, and the Electron Microscopy Facility at Curtin University.

REFERENCES CITED

Arana, A., and Cavosie, A.J., 2014, A study of shocked quartz in breccia from the Rock Elm impact structure: Houston, Texas, Lunar and Planetary Institute, Lunar and Planetary Science XXXXV, abstract 2185.

Cavosie, A.J., Quintero, R.R., Radovan, H.A., and Moser, D.E., 2010, A record of ancient cataclysm in modern sand: Shock microstructures in detrital minerals from the Vaal River, Vredefort Dome, South Africa: Geological Society of America Bulletin, v. 122, p. 1968–1980, doi:10.1130/B30187.1.

Chen, M., Yin, F., Li, X., Xie, X., Xiao, W., and Tan, D., 2013, Natural occurrence of reidite in the Xiuyan crater of China: Meteoritics & Planetary Science, v. 48, p. 796–805, doi:10.1111/maps.12106.

Cordua, W.S., 1985, Rock Elm structure, Pierce County, Wisconsin: A possible cryptoexplosion structure: Geology, v. 13, p. 372–374, doi:10.1130/0091-7613(1985)13<372:RESPCW>2.0.CO;2.

Dutta, R., and Mandal, N., 2012, Structure, elasticity and stability of reidite ($ZrSiO_4$) under hydrostatic pressure: A density functional study: Materials Chemistry and Physics, v. 135, p. 322–329, doi:10.1016/j.matchemphys.2012.04.052.

Erickson, T.M., Cavosie, A.J., Moser, D.E., Barker, I.R., and Radovan, H.A., 2013a, Correlating planar microstructures in shocked zircon from the Vredefort Dome at multiple scales: Crystallographic modeling, external and internal imaging, and EBSD structural analysis: The American Mineralogist, v. 98, p. 53–65, doi:10.2138/am.2013.4165.

Erickson, T.M., Cavosie, A.J., Moser, D.E., Barker, I.R., Radovan, H.A., and Wooden, J., 2013b, Identification and provenance determination of distally transported, Vredefort-derived shocked minerals in the Vaal River, South Africa using SEM and SHRIMP-RG techniques: Geochimica et Cosmochimica Acta, v. 107, p. 170–188, doi:10.1016/j.gca.2012.12.008.

Evans, T.J., Cordua, W.S., and LePain, D.L., 2007, Preliminary geology of the buried bedrock surface, Pierce County, Wisconsin: Wisconsin Geological and Natural History Survey Open-File Report 2007–08.

French, B.M., Cordua, W.S., and Plescia, J.B., 2004, The Rock Elm meteorite impact structure, Wisconsin: Geology and shock-metamorphic effects in quartz: Geological Society of America Bulletin, v. 116, p. 200–218, doi:10.1130/B25207.1.

Glass, B.P., and Liu, S., 2001, Discovery of high-pressure $ZrSiO_4$ polymorph in naturally occurring shock-metamorphosed zircons: Geology, v. 29, p. 371–373, doi:10.1130/0091-7613(2001)029<0371:DOHPZP>2.0.CO;2.

Glass, B.P., Liu, S., and Leavens, P.B., 2002, Reidite: An impact-produced high-pressure polymorph of zircon found in marine sediments: The American Mineralogist, v. 87, p. 562–565.

Gucsik, A., Koeberl, C., Brandstätter, F., Libowitzky, E., and Reimold, W.U., 2004, Cathodoluminescence, electron microscopy, and Raman spectroscopy of experimentally shock metamorphosed zircon crystals and naturally shocked zircon from the Ries impact crater. In: Cratering in marine environments and on ice, Dypvik, H., Claeys, P., and Burchell, M. (Eds.), Springer, Heidelberg.

Knittle, E., and Williams, Q., 1993, High-pressure Raman spectroscopy of $ZrSiO_4$: Observation of the zircon to scheelite transition at 300 K: The American Mineralogist, v. 78, p. 245–252.

Kusaba, K., Syono, Y., Kikuchi, M., and Fukuoka, K., 1985, Shock behavior of zircon: Phase transition to scheelite structure and decomposition: Earth and Planetary Science Letters, v. 72, p. 433–439, doi:10.1016/0012-821X(85)90064-0.

Kusaba, K., Yagi, T., Kikuchi, M., and Syono, Y., 1986, Structural considerations on the mechanism of the shock-induced zircon-scheelite transition in $ZrSiO_4$: Physics and Chemistry of Solids, v. 47, p. 675–679, doi:10.1016/0022-3697(86)90082-X.

Leroux, H., Reimold, W.U., Koeberl, C., Hornemann, U., and Doukhan, J.-C., 1999, Experimental shock deformation in zircon: A transmission electron microscopic study: Earth and Planetary Science Letters, v. 169, p. 291–301, doi:10.1016/S0012-821X(99)00082-5.

Lovell, T.R., and Bowen, B.B., 2013, Fluctuations in sedimentary provenance of the Upper Cambrian Mount Simon sandstone, Illinois Basin, United States: The Journal of Geology, v. 121, p. 129–154, doi:10.1086/669230.

Lugo, C.M., and Cavosie, A.J., 2014, First report of shocked zircon at the Santa Fe impact structure (USA): Houston, Texas, Lunar and Planetary Institute, Lunar and Planetary Science XXXXV, abstract 1839.

Melosh, H.J., 1989, Impact Cratering: A Geologic Process: Oxford, UK, Oxford University Press, 245 p.

Moser, D.E., Cupelli, C.L., Barker, I.R., Flowers, R.M., Bowman, J.R., Wooden, J., and Hart, R.J., 2011, New zircon shock phenomena and their use for dating and reconstruction of large impact structures revealed by electron nanobeam (EBSD, CL, EDS) and isotopic U-Pb and (U-Th)/He analysis of the Vredefort Dome: Canadian Journal of Earth Sciences, v. 48, p. 117–139, doi:10.1139/E11-011.

Reid, A.F., and Ringwood, A.E., 1969, Newly observed high pressure transformations in Mn_3O_4, $CaAl_2O_4$, and $ZrSiO_4$: Earth and Planetary Science Letters, v. 6, p. 205–208, doi:10.1016/0012-821X(69)90091-0.

Spray, J., and Elliott, B., 2015, Earth Impact Database: Planetary and Space Science Centre, University of New Brunswick, Canada: http://www.passc.net/EarthImpactDatabase/, (accessed January 2015).

Stöffler, D., and Grieve, R.A.F., 2007, Impactites, *in* Fettes, D., and Desmons, J., eds., Metamorphic Rocks: A Classification and Glossary of Terms, Recommendations of the International Union of Geological Sciences: Cambridge, UK, Cambridge University Press, p. 82–92.

Thomson, O.A., Cavosie, A.J., Moser, D.E., Barker, I., Radovan, H.A., and French, B.M., 2014, Preservation of detrital shocked minerals derived from the 1.85 Ga Sudbury impact structure in modern alluvium and Holocene glacial deposits: Geological Society of America Bulletin, v. 126, p. 720–737, doi:10.1130/B30958.1.

Timms, N.E., Reddy, S.M., Healy, D., Nemchin, A.A., Grange, M.L., Pidgeon, R.T., and Hart, R., 2012, Resolution of impact-related microstructures in lunar zircon: A shock-deformation mechanism map: Meteoritics & Planetary Science, v. 47, p. 120–141, doi:10.1111/j.1945-5100.2011.01316.x.

Valley, J.W., Cavosie, A.J., Ushikubo, T., Reinhard, D.A., Lawrence, D.F., Larson, D.J., Clifton, P.H., Kelly, T.F., Wilde, S.A., Moser, D.E., and Spicuzza, M.J., 2014, Hadean age for a post-magma-ocean zircon confirmed by atom probe tomography: Nature Geoscience, v. 7, p. 219–223, doi:10.1038/ngeo2075.

van Westrenen, W., Frank, M.R., Hanchar, J.M., Fei, Y., Finch, R.J., and Zha, C.-S., 2004, In situ determination of the compressibility of synthetic pure zircon ($ZrSiO_4$) and the onset of the zircon-reidite phase transition: The American Mineralogist, v. 89, p. 197–203.

Wittmann, A., Kenkmann, T., Schmitt, R.T., and Stöffler, D., 2006, Shock-metamorphosed zircon in terrestrial impact craters: Meteoritics & Planetary Science, v. 41, p. 433–454, doi:10.1111/j.1945-5100.2006.tb00472.x.

Wittmann, A., Reimold, W.U., Schmitt, R.T., Hecht, L., and Kenkmann, T., 2009, The record of ground zero in the Chesapeake Bay impact crater- suevites and related rocks: Geological Society of America. Special Paper, v. 458, p. 349–376, doi:10.1130/2009.2458(16).

FIGURE CAPTIONS

Figure 1. Information for Rock Elm Breccia sample 13RE07. A: Simplified geologic map (after Evans et al., 2007). Cm = Cambrian Mount Simon sandstone. Middle Ordovician units, from oldest to youngest, include Opd (Prairie du Chien dolomite), Owr (Washington Road sandstone), and Ore (Rock Elm shale). B: Cut rock slab of breccia 13RE07. C: Quartz grain with planar fractures, sample 13RE07 (from Arana and Cavosie, 2014).

Figure 2. Shocked zircons in Rock Elm breccia. A: Map of zircon 36, showing crystallographic orientation of host zircon and microtwin lamellae (with an inverse pole figure color scheme; microtwin lamellae are green). B: Phase map of zircon 9. C: Phase map of zircon 10. Data for A are superimposed on a greyscale map of EBSD pattern quality (band contrast).

Figure 3. Images and crystallographic data of reidite-bearing zircon grain 9 (shown in Fig. 2B). A: Atomic number contrast image. B: Detail of inset from A showing (i) lamellar reidite, (ii)

nano-granular reidite in voids, and (iii) nano-granular reidite decorating the external surface. C: Map showing crystallographic misorientation across the host zircon, relative to a reference point (red cross). D: Map showing crystallographic orientation of reidite grains and lamellae (with an inverse pole figure color scheme; zircon is gray in this image). E: Pole figures for the host zircon and reidite forms (all are lower hemisphere, equal area stereographic projections). Data for C and D are superimposed on greyscale maps of EBSD pattern quality (band contrast).

[1]GSA Data Repository item 2015xxx, analytical methods, EBSD conditions, and additional images, is available online at www.geosciety.org/pubs/ft2015.htm, or on request from editing@geosociety.org or Documents Secretary, GSA, P.O. Box 9140, Boulder, CO 80301, USA.

Figure 1
Click here to download Figure: Figure1.pdf

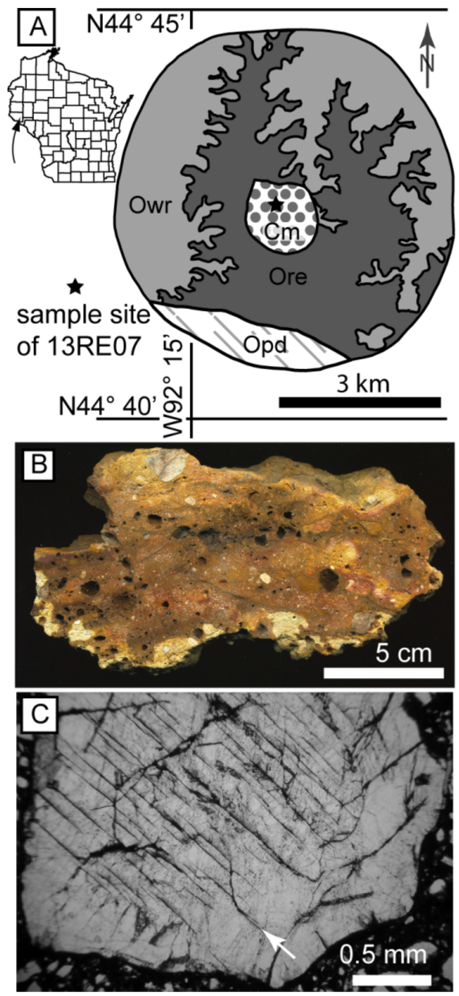

Figure 1

height = 30.5 pica
width =14 pica (1 col in 3 col layout)

Figure 2
Click here to download Figure: Figure2.pdf

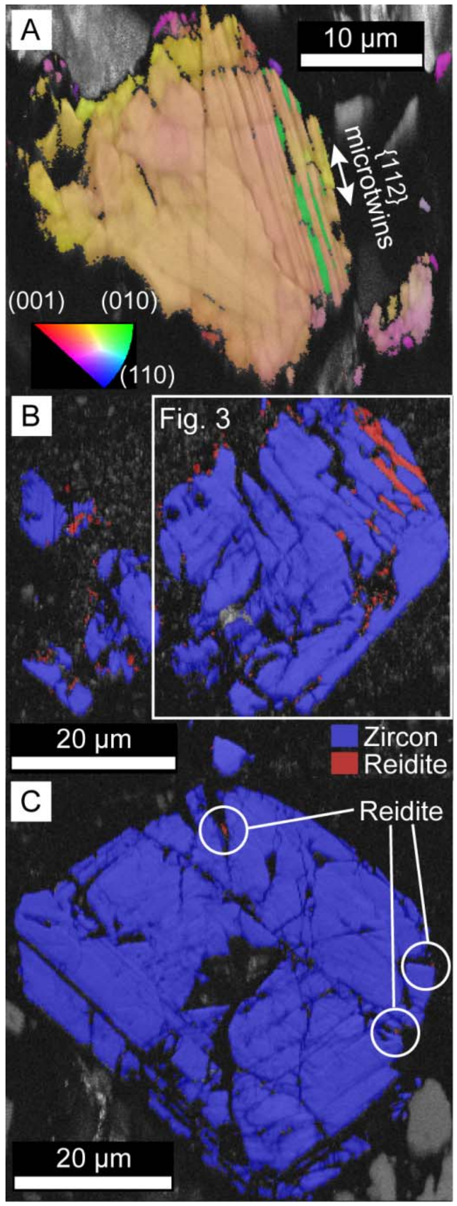

Figure 2

height = 37.5 pica
1 col width (14 pica) in 3 col layout

Figure 3
Click here to download Figure: Figure3.pdf

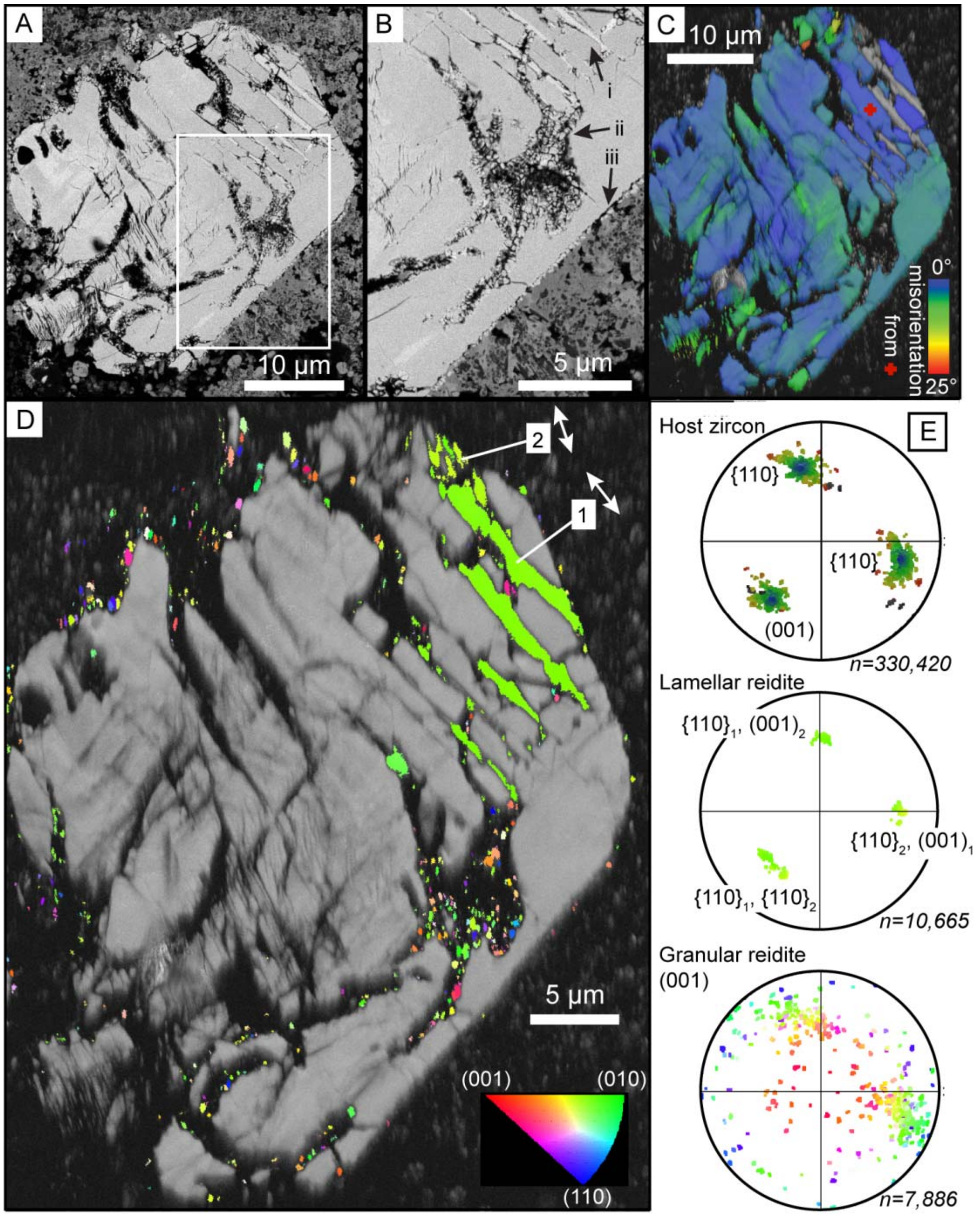

Figure 3

height = 38 pica
2 col width (29 pica) in 3 col layout

Data Repository Item. Analytical methods.

PETROGRAPHY. A thin section cut from sandstone breccia sample 13RE07 was first analyzed using transmitted light microscopy with a Leica DM EP petrographic microscope. This method allowed the identification of shock microstructures in quartz grains, and documentation of lithic clasts. Zircons were found to primarily occur as loose grains in the matrix, although a few were noted within clasts. The matrix is comprised of sand-sized grains of quartz and alkali feldspar, as well as fine-grained clay. Many grains are pervasively stained with a dark red-orange cement that renders many them opaque in transmitted light (Fig. DR1). Many of the clasts appear to be sedimentary in origin, consisting largely of quartz and clay; banding (layering?) is present in some. Some clasts were clay-rich and quartz-poor, while others appeared to be sandstone. No clasts could be confidently identified as igneous or metamorphic rocks; all appeared consistent with having been derived from the Mt. Simon sandstone or a lithological similar unit. No carbonate clasts were observed. The only shock microstructures identified in quartz were planar fractures (PDFs were not observed). The planar fractures are closely spaced (5-40 μm) and occur in parallel sets in different crystallographic orientations and are remarkably similar to cleavage in other minerals. Individual fractures appear to be open, and not filled with secondary material. Nearly identical planar microstructures were documented in quartz grains from samples of Rock Elm breccia by French et al. (2004) (see their Fig. 3).

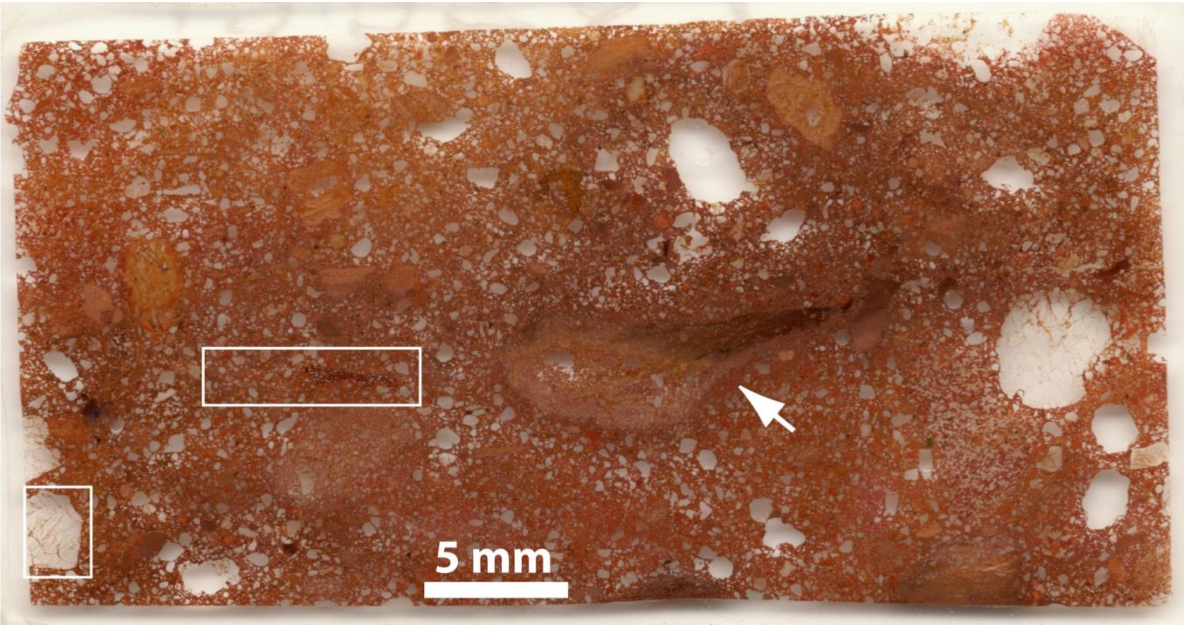

Figure DR1. Scan of the analyzed thin section (sample 13RE07). The white box along the lower-left edge of the section shows the location of the shocked quartz grain shown in Figure 1C. The larger white box to the left of center shows the region where zircons 9, 10, and 36 were found. The white arrow points to a deformed lithic clast.

SCANNING ELECTRON MICROSCOPY. The same section was analyzed using a Hitachi 3400S W-filament scanning electron microscope (SEM) at the University of Wisconsin-Madison. Standard SEM methods, including secondary electron (SE) and backscatter electron (BSE) imaging, and energy dispersive spectroscopy (EDS), were used with operating conditions of 15 kV and variable apertures.

High spatial resolution SEM analysis was conducted using a Tescan MIRA3 field emission gun (FEG) SEM at the Electron Microscopy Facility at Curtin University. The FEG-SEM was used for panchromatic cathodoluminescence (CL) imaging, and EBSD, and used SEM conditions and acquisition settings for zircon and reidite that followed closely those described in Erickson et al. (2015), and are summarized briefly here. Automated EBSD maps of regions of interest were generated by indexing of electron backscatter diffraction patterns on user-defined grids, and were collected for zircons 9, 10, and 36. Maps included both whole-grain analyses at ~0.2 µm step size and high resolution (0.05 µm step size) specific areas of interest. EBSD analyses were collected with a 20 kV accelerating voltage, 70° sample tilt, 20.5 mm working distance, and 18 nA beam intensity (Table 1). Electron backscatter patterns were collected with a Nordlys Nano high resolution detector and Oxford Instruments Aztec system using routine data acquisition and noise reduction settings (Table 1; Reddy et al., 2007). EBSD maps and pole figures were processed using the Tango and Mambo modules in the Oxford Instruments/HKL Channel 5 software package.

Grain size statistics of the nanoparticulate reidite were quantified using the Tango module in Channel5 software package of Oxford Instruments/HKL. Initially, noise reduction involved infill of isolated zero solution pixels with an average orientation based on a seven nearest neighbor extrapolation. Grains were identified automatically from a subset of the map that excluded the lamellar reidite, and was based on an orientation threshold of 10°. Only grains greater than 75 nm (i.e., 1.5 pixels) in diameter were then considered in the final statistics to remove the effects of potentially erroneous isolated data points.

REFERENCES

French, B.M., Cordua, W.S., and Plescia, J.B., 2004, The Rock Elm meteorite impact structure, Wisconsin: Geology and shock-metamorphic effects in quartz: Geological Society of America Bulletin, v. 116, p. 200–218, doi:10.1130/B25207.1.

Reddy, S.M., Timms, N.E., Pantleon, W., and Trimby, T., 2007, Quantitative characterization of plastic deformation of zircon and geological implications: Contributions to Mineralogy and Petrology v. 153, p. 625-645.

Data Repository item. EBSD analytical conditions.

EBSD analysis conditions.

SEM Model	Tescan Mira3 FEG-SEM				
Grain	Zircon 36	Zircon 9	Zircon 9	Zircon 10	Zircon 10
Show in figure	2A, DR	2B	3C, 3D	2C	DR
Acquisition speed (Hz)	22.42	22.29	22.53	40.01	21.92
Background (frames)	64	64	64	64	64
Binning	2x2	2x2	2x2	4x4	2x2
Gain	High	High	High	High	High
Hough resolution	60	60	60	60	60
Band detection min/max	6/8	6/8	6/8	6/8	6/8
Average mean angular deviation (zircon)	0.80	0.61	0.62	0.60	0.65
X steps	369	276	727	285	136
Y steps	326	247	919	270	344
Step distance (nm)	50	200	50	200	50
Noise reduction – ‘wildspike’	Yes	Yes	Yes	Yes	Yes
n neighbour zero solution extrapolation	0	0	0	0	0
Kuwahara Filter	No	No	No	No	No
Tescan Mira3 FEG-SEM settings					
EBSD system	Nordlys Detector - Aztec				
Carbon coat (<5nm)	Yes	Yes	Yes	Yes	Yes
Acc. voltage (kV)	20	20	20	20	20
Working distance (mm)	20.5	20.5	20.5	20.5	20.5
Tilt (degrees)	70	70	70	70	70

DR = Data Repository

Data Repository Item. Additional images of zircon 36. A: Back-scattered electron image of zircon 36 showing variations in average atomic number. B: Map showing crystallographic misorientation across zircon 36, relative to the red cross (near bottom of grain). C: Map showing crystallographic orientation of zircon 36 (with an inverse pole figure color scheme). Twins appear as green lamellae on right side of grain. D: Pole figures for the host zircon and microtwins (labeled).

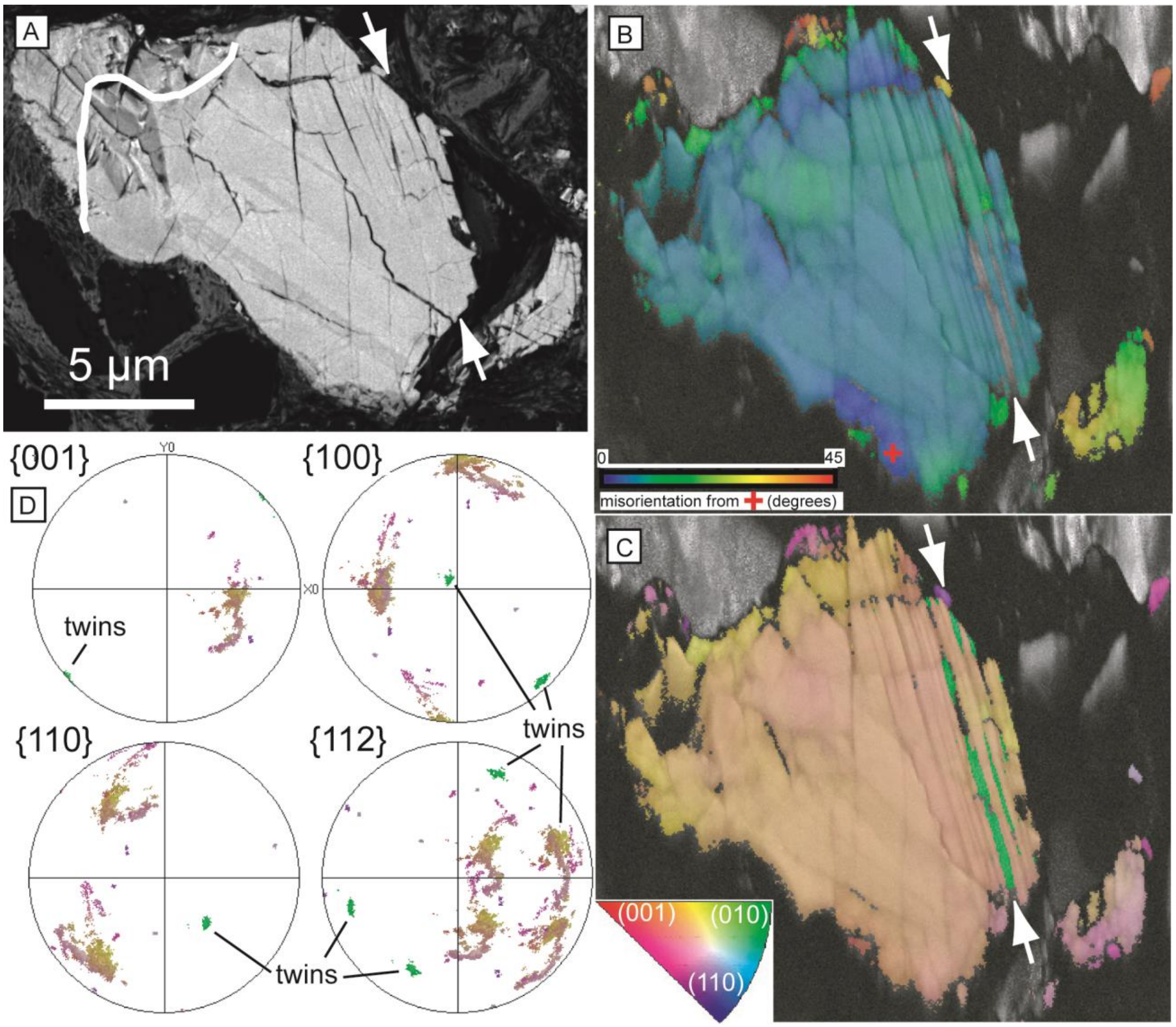

Data Repository Item. Additional images of zircon 9. A: Back-scattered electron image showing variations in average atomic number; lamellar reidite (brighter) is indicated by black arrow. B: Cathodoluminescence image showing how reidite are non-luminescent (see white arrow), and cross-cut growth zoning. The oscillatory zoned core is labeled.

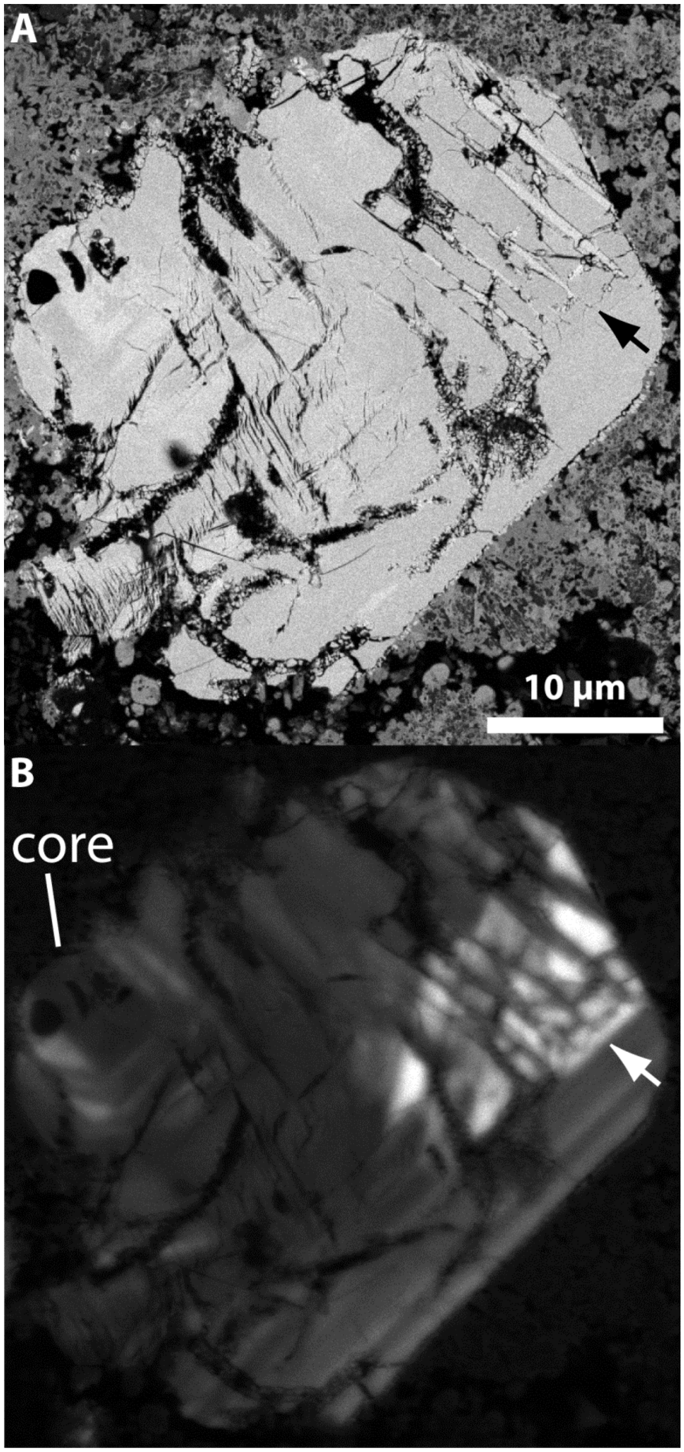

Data Repository Item. Additional images of zircon 10. A: Back-scattered electron image showing variations in average atomic number. B: CL image. C: Phase map. D: Map showing crystallographic orientation (with an inverse pole figure color scheme). E: Map showing crystallographic misorientation, relative to the red cross (near top of grain). F,G,H: Close-up maps of a reidite domain from inset in C (images as in C,D,E). I. Pole figures for the host zircon and reidite.